Investigation of safety related ignition processes of laminar strained premixed stoichiometric NH_3-H_2-air flames⋆

Chunkan Yu[a,*], Sven Eckart[b], Stefan Essmann[c], Detlev Markus[c], Agustin Valera-Medina[d], Robert Schießl[a], Bo Shu[c], Hartmut Krause[b] and Ulrich Maas[a]

[a] *Institute of Technical Thermodynamics, Karlsruhe Institute of Technology, Engelbert-Arnold-Str. 4, Karlsruhe 76131, Germany*
[b] *Institute of Thermal Engineering, TU Bergakademie Freiberg, Freiberg, Germany*
[c] *Physikalisch-Technische Bundesanstalt (PTB), Braunschweig, Germany*
[d] *College of Physical Sciences and Engineering, Cardiff University, Cardiff CF24 3AA, United Kingdom*

ARTICLE INFO

Keywords:
hazards
ammonia
industrial explosions
spark ignition
strained premixed flame

ABSTRACT

The ignition properties of ammonia (NH_3) / hydrogen (H_2) mixtures are important because of their abundance in chemical engineering processes, and also because of their prospective role as fuels in future energy systems. In particular, the question arises if and how important characteristics like ignition limits and minimum ignition energies in NH_3/H_2 mixtures are related to the physical conditions . To address these questions, this work studies ignition process in ammonia/hydrogen mixtures by numerical simulations. These track the evolution of ammonia/hydrogen mixtures during and after the deposition of a certain ignition energy, using a detailed treatment of chemical reactions and molecular transport. Studies on the influence of initial and boundary conditions on the minimally required ignition energy are performed. These are the strain rate, hydrogen content, pressure and initial (pre-ignition) temperature. Significant findings include a sharp, linear correlation between the transition strain rate, defined as the strain rate below which no external energy is required to initiate successful ignition (auto-ignition) and a characteristic reaction time, defined as the inverse of ignition delay time in homogeneous, quiescent mixtures. Also, the relative decay of minimum ignition energy with increasing hydrogen content is less pronounced for higher pressures. Analysis of the results supports a knowledge-based approach towards fail-proof ignition devices and reliable prevention of hazards. The simulations are used for assessing the ignitability of ammonia and its mixtures with hydrogen.

1. Introduction

Spark ignition is an important aspect of fundamental and applied combustion research. It typically involves a complex interaction of physical and chemical processes. For example, flame initiation and propagation is impaired in mixtures with Lewis numbers above unity ($Le > 1$). Compared to $Le = 1$, more ignition energy must therefore be applied to trigger successful ignition. Also, induced flow fields can interfere more strongly with the ignition process for $Le > 1$ compared to $Le = 1$, leading to a larger degree of variation in the ignition process (Essmann et al., 2020). Therefore, flame propagation for mixtures with a Lewis number considerably above unity can be dominated by flow effects (spark assisted flame propagation) during the critical phase (Bradley and Lung, 1987).

While spark ignition processes have been studied for various hydrocarbon fuels under a wide range of conditions, the knowledge base on spark ignition in ammonia is still scarce. This contrasts with the increasing interest on ammonia as a carbon-free fuel (see e.g.Valera-Medina et al. (2018) for an overview).

The reactivity of pure ammonia is generally low, causing it to be prone to flame blow-off. Also, the minimum ignition energy required to burn ammonia/air mixtures is by orders of magnitude higher than that of, e.g., hydrogen cite whom???

Also, the laminar burning velocity of ammonia/air mixtures is significantly lower than that of e.g., hydrogen (Ichikawa et al., 2015).

⋆This document is the result of the research project funded by the Deutsche Forschungsgemeinschaft (DFG).

*Corresponding author. Institute of Technical Thermodynamics, Karlsruhe Institute of Technology, Engelbert-Arnold-Str. 4, Karlsruhe 76131, Germany
chunkan.yu@kit.edu (C. Yu)
ORCID(s):

Thus, adding hydrogen is a common way to improve the ignitability and general combustion properties of ammonia (Li et al., 2021). Addition of hydrogen to ammonia mixtures can, more generally, enhance combustion properties, e.g., yield higher flame speeds. At sufficient hydrogen addition levels, ammonia fuel may exhibit a lower propensity of flame extinction compared to a methane/air flame (Wiseman et al., 2021). Ammonia/hydrogen mixtures can also readily be produced on a large scale, e.g., by partial cracking of ammonia (Abbas and Daud, 2010), or also directly be obtained from ammonia production processes by incomplete conversion of the initial nitrogen/hydrogen mixture.

A particularly complicated (and particularly important) configuration occurs when an ignition event is embedded into a turbulent flow. High turbulence intensities impose high strain rates on the flow, and, as a general tendency, achieving successful ignition is more difficult in flows with higher strain rates Huang et al. (2007); De Soete (1971); Shy et al. (2017). For the development of practical devices, it is therefore important to assess how ignition in hydrogen/ammonia mixtures reacts to strain rate.

The present work focuses on investigating safety-related ignition process of ammonia/air mixtures with different level of H_2 addition. The investigation is based on numerical simulations involving detailed treatment of chemical reaction and transport, on the influence of strain rate and pre-heat temperature on ignition is performed. From an analysis of the data, insight is gained that can support the development of reliable ignition systems and ignition-hazard proof devices dealing with ammonia/hydrogen mixtures.

The paper is structured as follows: First, details of the model and its numerical implementation are explained, and a validation of simulations against published experimental data is given. Then, simulation data on the dependence of ignition characteristics on initial and boundary conditions are presented. Finally, the significance of these results for the design of devices that intend to initiate or to prevent ignition is discussed.

still more citations in intro? ... I moved some from results part to intro, where they seemed to fit better. e.g.: DNS of turbulent NH3/H2/N2 flames (A. Gruber et al),

2. Modeling and numerical method

The physical model used fore the study is presented in Fig.1. A strained premixed flame is considered, where flows of premixed unburned gas impinge and mix, formation a stagnation point. Both flows have identical temperature, pressure and chemical composition, but different velocities relative to the stagnation point. In this system, an ignition energy is released at some spatial domain and for some time. Depending on the flow velocity, the system can lead to a stable flame or flame extinguish.

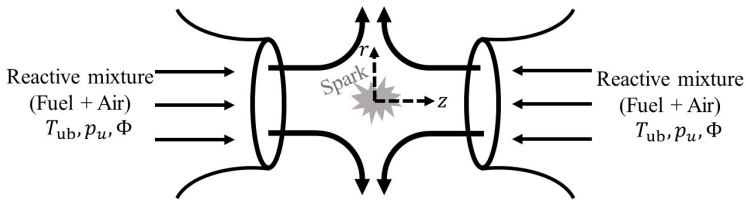

Figure 1: Schematic illustration of the strained premixed laminar flame.

We consider a one-dimensional flame in counterflow configuration, using a two-parameter formulation based on tangential pressure gradient J and radial velocity gradient G, as described in detail in Stahl and Warnatz (1991), to describe the flow field. This model depends only on one spatial variable (the z-axis, i.e., the flame surface normal direction) with infinite extent in the other two directions (slab geometry) with the domain $z \geq 0$ due to symmetry.

The strain rate describes the "strength" of the flow which is constant throughout the whole flow, and can be determined by means of the tangential pressure gradient J as (Stahl and Warnatz, 1991):

$$a = \sqrt{-\frac{J}{\rho_{ub}}}, \tag{1}$$

where ρ_{ub} is the density of the unburned gas.

The spark ignition energy is modelled using a prescribed spatio-temporal power density $\dot{q}_s$ according to Maas et al. (1988):

$$\dot{q}_s(z,t) = \begin{cases} \frac{D_s}{\tau_s} \cdot \exp\left[-\left(\frac{z}{\delta_W}\right)^8\right] & \text{for } 0 \le t \le \tau_s, \\ 0 & \text{otherwise.} \end{cases} \tag{2}$$

Here, D_s is the maximum energy density (J/m^3) at $z = 0$, and δ_W is the spark width. τ_s is the spark duration time describing how long the spark energy is provided into the system. Note that this reflects the spark energy of practical device, as shown in Maas et al. (1988), and no energy exists for $r \to \infty$. Based on $\dot{q}_s(z,t)$, one can also calculate the total deposited energy E_s per surface (in J/m^2), which can be determined as:

$$E_s = \int_{z=-\infty}^{+\infty} \int_{t=0}^{\tau_s} \dot{q}_s(z,t) \mathrm{d}t \mathrm{d}z = 2 \cdot D_s \cdot \delta_W \cdot \Gamma\left(\frac{9}{8}\right) \tag{3}$$

where $\Gamma(\cdot)$ is the gamma function ($\Gamma(9/8) \approx 0.94174$).

For the numerical simulation, the system of PDEs requires initial and boundary conditions for a unique solution. Initially, all the thermo-kinetic states such as temperature ($T(z,t)$) and species concentrations (mass fraction $w_i(z,t)$) are homogeneously distributed through the whole spatial domain. In other words, no spatial gradients of temperature and species concentrations exist:

$$T(z, t = 0) = T_{ub}, \quad w_i(z, t = 0) = w_{i,0}. \tag{4}$$

- Left boundary: we set the symmetry line ($z = 0$ in Fig.**??**) as the left boundary. Neumann boundary conditions are specified for temperature $T(z,t)$ and species concentrations $w_i(z,t)$: $\partial T/\partial z|_{z=0} = 0$, and $\partial w_i/\partial z|_{z=0} = 0$. The velocity is $v = 0$ because it corresponds to the stagnation point.
- Right boundary: Dirichlet boundary conditions are specified. Values of temperature $T = T_{ub}$ and species concentrations $w_i = w_{i,0}$ remain unchanged at any time here. Furthermore, a constant value of the tangential pressure gradient J is also specified here in order to define the strain rate imposed on the system (c.f. Fig.1).

Simulations are initialized with a homogeneous distribution of species mass fractions ($w_i(z, t = 0) = w_{i,ub}$) and temperature ($T(z, t = 0) = T_{ub}$), with index "ub" specifying the unburnt gas. The pressure for the present work is assumed to be constant during the whole spark and combustion processes with $p = 1$ bar. The constant pressure considered in the present work is a good approximation if the spark duration is longer than 0.01 ms (Maas et al., 1988). The left boundary is specified at the the symmetry axis ($z = 0$) where a Neumann condition (zero gradient) is applied for the species mass fractions and temperature, and the velocity is $v = 0$. On the right side, a Dirichlet boundary condition (fixed value) is used for species mass fractions and temperature. Furthermore, the tangential pressure gradient J is also given as input into the system for the specification of the strain rate imposed to the flame.

A detailed transport model including the thermal diffusion (Soret effect) (Hirschfelder et al., 1964) is considered in the simulation. Furthermore, the thermal radiation is neglected. However, it is worth studying the radiation effect on the NH_3 combustion system in the future.

The model is simulated numerically using the in-house code INSFLA (Maas and Warnatz, 1988). This code solves for the spatio-temporal evolution of the underlying system of PDEs for the given initial and boundary conditions using the method of lines. This involves an error-control based automatic adaptive time stepping.

2.1. Gas mixture and chemical mechanism

H_2-enriched stoichiometric ammonia/air mixtures, are considered in this study. The amount of H_2 is described by the mole fraction α_{H_2} of H_2 in the fuel:

$$\alpha_{H_2} H_2 + (1 - \alpha_{H_2}) NH_3 + \left(0.75 - \frac{\alpha_{H_2}}{4}\right)(O_2 + \frac{79}{21} N_2), \tag{5}$$

where Φ is the fuel/air equivalence ratio.

In this work, we focus on stoichiometric mixtures with varying H_2 content, as $0 \le \alpha_{H_2} \le 0.4$. This is motivated mainly by the following:

	mole fraction			
α_{H_2}	H_2	NH_3	O_2	N_2
0.0	0.0	0.2188	0.1641	0.6171
0.1	0.0225	0.2021	0.1628	0.6162
0.2	0.0462	0.1846	0.1615	0.6077
0.3	0.0712	0.1661	0.1602	0.6025
0.4	0.0977	0.1465	0.1587	0.5971
1.0	0.2958	0.0	0.1479	0.5563

Table 1
Mole fractions of species in stoichiometric NH_3-H_2-air mixtures

(i) previous works performed by Božo et al. (2019) have suggested the use of blends with less than 40% hydrogen concentration to maintain stable combustion in turbulent, swirling flames.

(ii) The work, expanded recently to various equivalence ratios (Mashruk et al., 2022), also suggests that the increase to 50% hydrogen leads to hydrogen overtaking the combustion profile, even creating two flame fronts (Valera-Medina et al., 2018; Goldmann and Dinkelacker, 2021).

(iii) Finally, with increasing hydrogen content, the high temperature hydrogen attack (HTHA) might become serious and destroy the material in real applications (Cesaro et al., 2021). This, in turn, leads to lower efficiencies.

Therefore, it was decided that values $0 \leq \alpha_{H_2} \leq 40\%$ would be investigated in the present work, as these would keep ammonia-based features whilst being more representative to future industrial systems working on ammonia/hydrogen blends. Pure ammonia gas ($\alpha_{H_2} = 0.0$) and pure hydrogen gas ($\alpha_{H_2} = 1.0$) are also considered as references, comparing the performance with the hydrogen-enriched ammonia. Tab.1 lists mole fractions of species concentrations for stoichiometric unburnt NH_3-H_2-air gas mixture for different H_2 addition levels (α_{H_2}).

To perform the numerical simulation, the Li-2019 detailed chemical mechanism is used for the numerical simulation of the considered combustion system (Li et al., 2019). This mechanism, which is originally designed for NH_3-H_2-CH_4 air combustion system, consists of 128 reactive species and 957 reactions and has been validated against recent literature experimental data such as ignition delay times, laminar burning velocities, and speciation. Good performance has been reported (Li et al., 2019). Removing all species including hydrocarbon and inertgas such as Ar and He, the remaining mechanism has 34 species and 252 reactions.

Figure 2 compares the predicted laminar burning velocities (S_L) with various experimental measurements of NH_3-H_2-air laminar premixed flames at 1 bar and an initial temperature of 298 K. In general, the chemical mechanism gives qualitatively good agreement. It should be emphasized that due to the low burning velocities of ammonia, the influence of buoyancy is more important, especially for the spherically expanding flames Hayakawa et al. (2015a). The few known experiments therefore vary in part by up to 50% from each other. Here we should mention that the over-prediction for some situations is also observed using other mechanisms, and reported in other literature Yin et al. (2022).

Figure 3 compares furthermore the predicted extinction strain rates (ESR) a_E with experiment measurements (Colson et al., 2016) of a NH_3-air strained premixed laminar flame at 1 atm and 5 atm. Good agreement can be observed, although the ESR at 5 atm is over-predicted.

2.2. Failed and successful ignition

For spark ignition scenarios, two qualitatively different outcomes are possible, namely a failure to ignite or a successful ignition, followed by a self-sustained flame propagation.

Fig.4 and 5 show representative spatial profiles for temperature- and mass fractions of NH_2 and HNO for a NH_3/H_2/air combustion system at different times during a failed and successful ignition, respectively. The red profiles correspond to times where ignition energy is still supplied, blue lines represent times after the ignition source has shut down. The tow cases differ only by the deposited energy: for failed ignition (Fig.4), $D_s = 310$ kJ/m^3, and for a successful ignition shown (Fig.5), $D_s = 320$ kJ/m^3 (corresponding to the minimum spark ignition energy $D_s^{\min}$ for a successful ignition). Temperature at the ignition location increases continuously during the spark duration, because the gas mixture is heated up through the ignition energy. After the spark duration time,

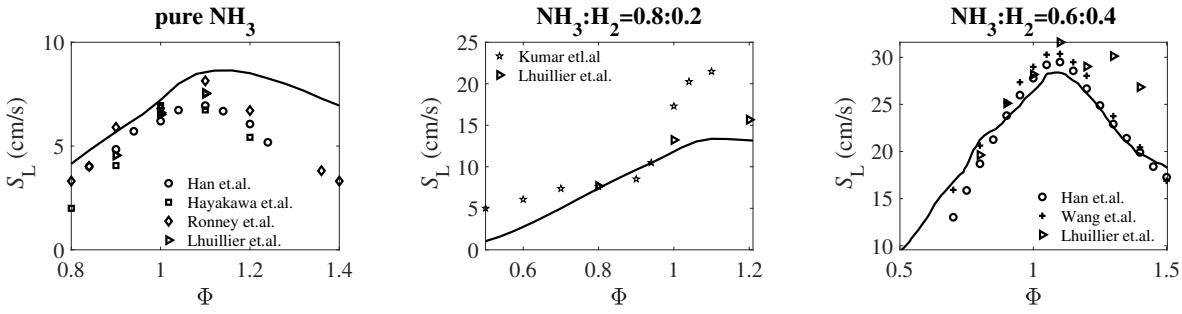

Figure 2: Comparison between simulation results and the measurements from Han et.al. (Han et al., 2019a,b), Hayakawa et.al.(Hayakawa et al., 2015b), Ronney et.al. (Ronney, 1988), Lhuillier et.al. (Lhuillier et al., 2020), Kumar and Meyer Kumar and Meyer (2013), Wang et.al. (Wang et al., 2020) for laminar burning velocities S_L of NH_3-H_2-air mixtures at 1 bar and an initial temperature of 298 K.

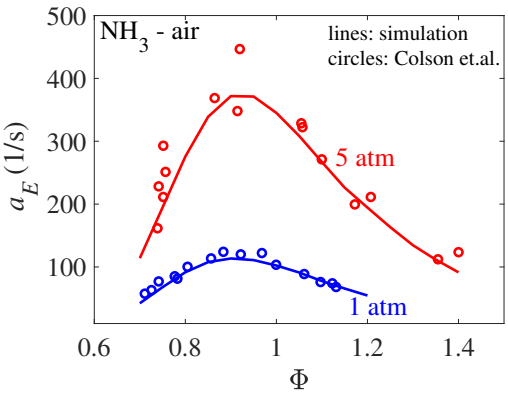

Figure 3: Comparison between simulation results and the measurements from Colson et al. (2016) for extinction strain rate a_E of a NH_3-air strained premixed laminar flame at 1 atm and 5 atm.

- for a failed SI (Fig.4), the temperature of the whole system is the same as the initial temperature (temperature is homogeneous distributed) at the steady state. The species such as NH_2 and HNO, which are shown here, are slightly produced and then consumed rapidly, such that no these intermediate species are produced at the steady state over the whole system domain.
- for.a successful SI (Fig.5), after a certain time we obtain a stable steady burning flame at steady state.

In the following discussion, we will focus on the minimum ignition energy density $D_s^{\min}$ required for a successful ignition. The effect of the amount of added co-fuel (H_2), the strain rate a, pressure p and the gas mixture temperature T_{ub} on the $D_s^{\min}$ will be investigated and discussed in detail.

3. Results and discussion

The effect of spark ignition parameters has been investigated in details with mathematical formulation in Ref.**??**, therefore in the present work, focus will be put on the effect of strain rate imposed in the flow, of the pressure of the combustion system and, especially, of the hydrogen content as co-fuel and of the gas mixture temperature. All the simulations are performed with spark width $\delta_w = 1$ mm and spark duration time $\tau_s = 1$ ms.

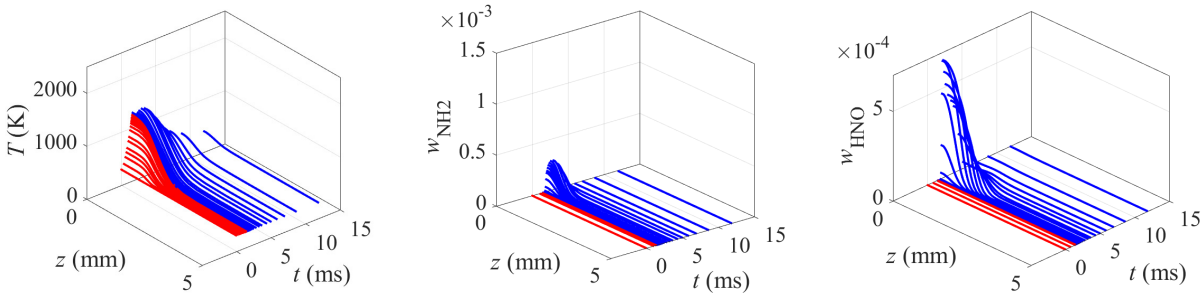

Figure 4: Time development of spatial profiles of temperature and selected species mass fractions for a typical failed spark ignition.

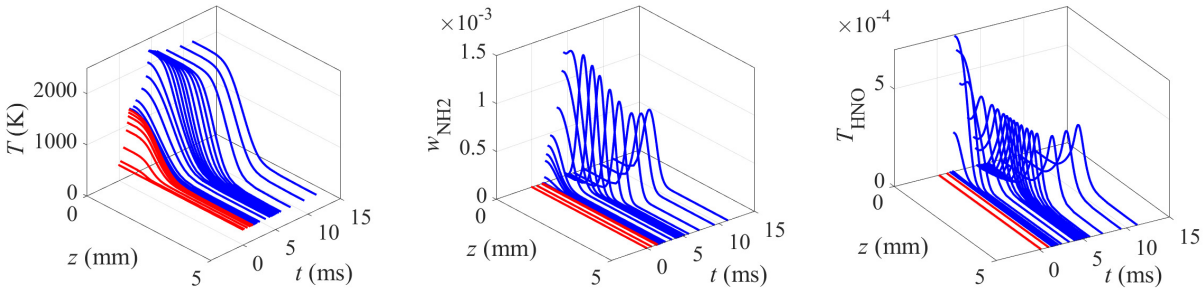

Figure 5: Time development of spatial profiles of temperature and selected species mass fractions for a typical successful spark ignition.

3.1. Effect of strain rate

Figure 6 shows the dependence of $D_s^{\min}$ on strain rate for stoichiometric mixture with different H_2 addition under pressure $p = 1$ bar. A monotonic increasing of $D_s^{\min}$ with increasing strain rate is observed here. Note that the tendency ends up at the extinction strain rate (ESR), above which no stable burning solution can be obtained. It can be clearly seen that the ESR increases with increasing H_2 content. Such tendency of the ESR is consistent with observed in e.g. Lee and Kwon (2011), and the effect of H_2 addition on ESR is beyond scope of this work. Note that, although it is not shown here, such tendency also holds for other system pressures. Such dependence can be attributed to two main reasons:

- the higher the strain rate is, the higher the flow velocity (and consequently the mass flux) is. Therefore, if the flow is imposed with higher strain rate, more unburned gas mixture per time unit passes the spark ignition regime. Therefore, at the end of the spark duration, the temperature becomes lower with increasing strain rate, as shown in Fig.7. Therefore, more spark energy must be provided to heat up the unburned gas mixture for flow with increasing strain rate.

- the higher the strain rate is, the higher the rate of energy transport (convection and heat conductivity) is: high convection due to high flow velocity; and high rate of heat conductivity due to high spatial gradient of temperature. Therefore more spark energy must be provided with increasing strain rates to compensate increasing rate of energy transport.

In practical combustion devices, flows with higher turbulence intensity impose higher strain rates, indicating that more spark energy is required for flows with higher turbulence. This is also observed in e.g. Huang et al. (2007); De Soete (1971); Shy et al. (2017).

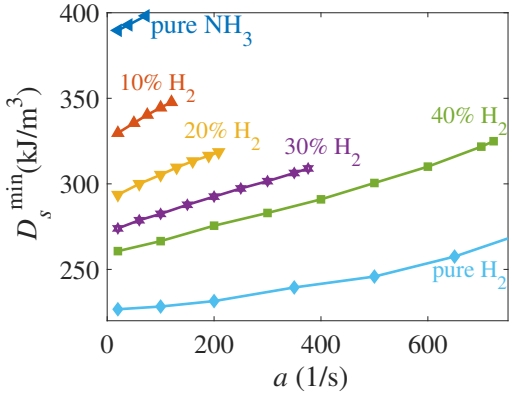

Figure 6: Dependence of the $D_s^{\min}$ against strain rate for different levels of H_2 in the fuel. Igniter: $\delta_w = 1$mm and $\tau_s = 1$ms; $p = 1$bar, $T_{\text{ub}} = 300$K.

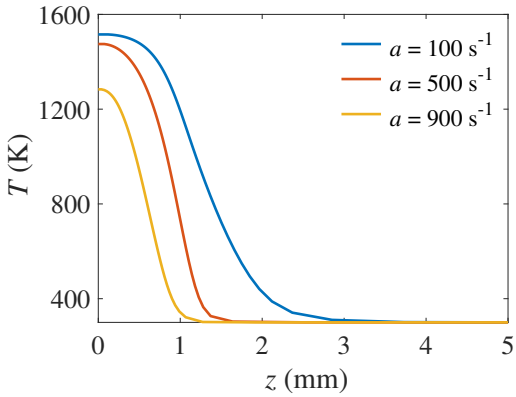

Figure 7: The temperature profiles at $t = \tau_s$ for flows with different strain rates under $p = 1$ bar for stoichiometric mixture with NH_3:H_2=0.9:0.1. Unburnt mixture gas temperature: $T_{\text{ub}} = 300$K. Spark energy density $D_s^{\min} = 345$ kJ/m^3.

3.2. Effect of hydrogen content

In this section, we investigate the effect of H_2 content in the gas mixture on the ignition energy, as listed in Tab.1. Besides the Fig. 6 where one compares the $D_s^{\min}$ over strain rate for different levels of H_2 addition, Fig.8 shows the dependence of $D_s^{\min}$ on H_2 content for three different pressures under the same flow strain rate, and the Fig.9 shows further the relative deviations $\frac{D_s^{\min}}{D_s^{\min}(\text{pure } H_2)}$.

We observe that the pure NH_3-air gas mixture required much higher spark energy. For example, at 10 bar and 20 bar, the $D_s^{\min}$ of pure NH_3-air is around 20% higher than the $D_s^{\min}$ of mixture with 10% H_2 addition, and around 20% higher than the $D_s^{\min}$ of pure H_2-air mixture. Such fact that the pure NH_3-air mixture is difficult to be ignited has also been confirmed in many other study REFERENCES.

Focusing on the H_2-enriched ammonia gas mixture, we observe a clear monotonic decrease of the $D_s^{\min}$ with increasing H_2-content. This is because of the two main reasons:

- the heat capacity decreases with increasing H_2 content, therefore less energy is required for the system to reach sufficiently high temperatures required for a successful ignition;
- with the increasing of H_2 content in the gas mixture, the chemical reactions become faster and the gas mixtures can be self-ignited faster after removing the spark.

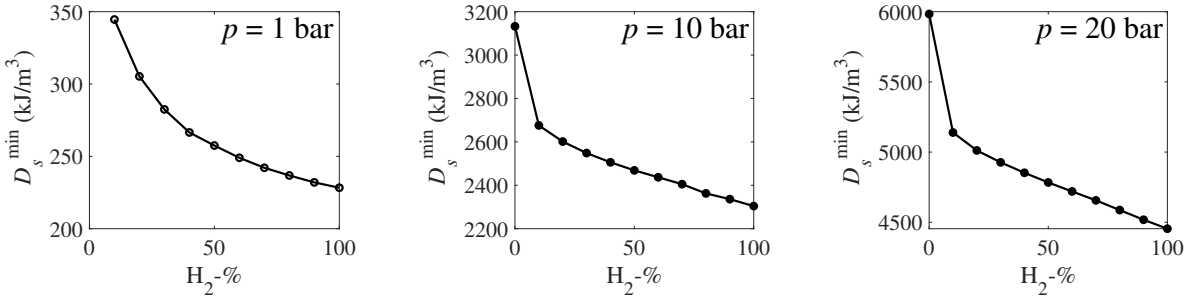

Figure 8: Dependence of the $D_s^{\min}$ on different levels of H_2 in the fuel for different pressures. Flow strain rate: $a = 100\text{s}^{-1}$; $T_{\text{ub}} = 300\text{K}$.

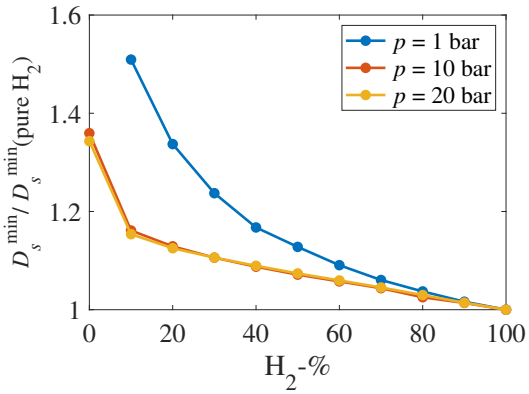

Figure 9: Dependence of the $D_s^{\min}/D_s^{\min}(\text{pure } H_2)$ on the pressure for flow imposed with strain rate $a = 100\text{s}^{-1}$. $T_{\text{ub}} = 300\text{K}$.

3.3. Effect of pressure

Figure 9 discussed above shows that the addition of H_2 at $p = 1$ bar can largely reduce the $D_s^{\min}$, while the addition of H_2 at $p = 10$ bar and 20 bar becomes less effective to reduce the $D_s^{\min}$. Here we must find out some reasons. Check IDT. Such effect can be reflected in the ignition delay of ammonia-hydrogen mixtures at elevated pressures, as reported in He et al. [ref, He CnF 2019] the addition of small amount of hydrogen in ammonia (e.g., 1 and 5 percent) at 20 and 40 bar can significantly reduce the IDT of the gas mixtures, however, the efficiency of hydrogen addition of 10 and 20 percent is much weaker and the IDT of ammonia-hydrogen mixtures which contain hydrogen more than 20 percent are very close to the pure hydrogen

Figure 10 shows the influence of the pressure on the $D_s^{\min}$. The flow is imposed with strain rate $a = 100\text{s}^{-1}$, which is considered as representative example. The numerical results here show that the $D_s^{\min}$ increases with increasing pressure, which is consistent to the statement in Maas and Warnatz (1988). This is attributed to the fact that, as stated in Maas and Warnatz (1988), higher pressures correspond to higher heat capacities inside the spark volume, leading to an increase of required spark ignition energies.

3.4. Pre-heating: Gas mixture temperature

Figure 11 shows $D_s^{\min}$ against strain rate for various initial gas temperatures. It is straightforward and also well known that with increasing gas temperatures, gas needs less spark ignition energy to be heated up to reach the necessary ignition temperature. However, if we further increase the gas temperature, we would expect that the gas mixture can be

(i) self-ignited due to its sufficient high temperature (correspondingly short ignition delay times), or

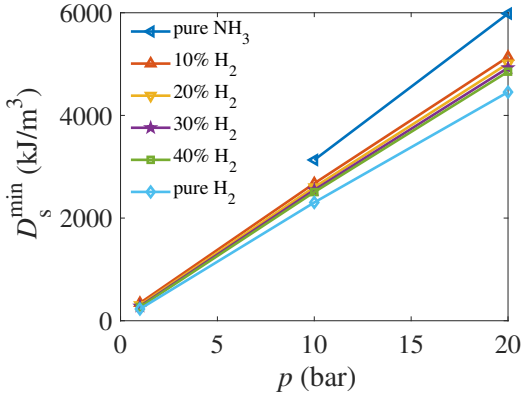

Figure 10: Dependence of the D_s^{min} on the pressure for flow imposed with strain rate $a = 100\text{s}^{-1}$. $T_{ub} = 300$K.

(ii) forced ignited only we provide the external spark energy, depending on the flow strength.

This can be observed through the blue line in Fig.11, where the initial gas temperature is T_{ub} =1000 K: at low strain rate regime (here $a < 674$ s^{-1}), no external spark energy is required ($D_s^{min} = 0$) and the gas mixture can self-ignite due to its own fast reaction rate; at high strain rate regime (here $a > 674$ s^{-1}) the external spark energy is required to force the gas mixture to be ignited. As we observe, there exists a so-called transition strain rate a_{trans} which distinguishes between the self ignition and the spark ignition.

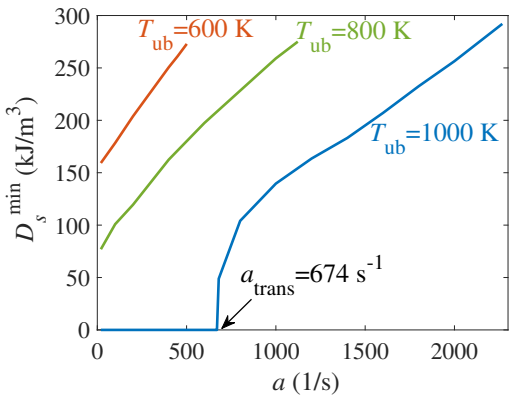

Figure 11: CHANGE !!! The dependence of D_s^{min} on gas temperature T_{ub} for flames under $p = 1$ bar. Stoichiometric gas mixture with NH_3:H_2=0.9:0.1. Igniter parameter: δ_w = 1mm, τ_s =1 ms.

Since the gas mixture with sufficient temperatures can be self-ignited rapidly, the characteristic reaction rate $k(T_{ub})$ at T_{ub}, which is defined as the inverse of the ignition delay time, can be introduced:

$$k(T_{ub}) = \frac{1}{\tau_{ign}(T_{ub})}. \tag{6}$$

This characteristic reaction rate is a suitable quantity to measure how fast the reaction of a combustion system takes place, which was discussed in detail in Livengood and Wu (1955).

The dependence of a_{trans} on the gas temperature T_{ub} is represented in Fig.12 for different levels of H_2 addition and pure H_2 and pure NH_3 gas mixture at normal and elevated pressures. In order to clarify the physical meanings, the characteristic reaction rates $k(T_{ub})$ over the considered gas temperature regimes are also represented in Fig.13. The

first straightforward observation is that the pure NH_3-air has a very low a_{trans} for all considered pressures. This is attributed to the fact that for a pre-heated pure NH_3-air gas mixture, it can be very difficult to achieve self-ignition due to its low reaction rate (c.f. blue lines in Fig.13) and burning rate (Valera-Medina et al., 2019). A reliable combustion is achievable only when one provides external spark ignition. From the other side, the pure NH_3-air gas mixture has the lowest possibility of hazardous explosion danger.

The phenomenon becomes more complicated if the ammonia is mixed with hydrogen. As we observe from Fig.12, for mixtures with 10% and 20% H_2 enrichment, the pressures promote the reaction rates and consequently the self-ignition against the flow strain rate for the considered temperatures, and the a_{trans} increases with increasing pressure monotonically. However, the a_{trans} and $k(T_{ub})$ change non-monotonically with the pressures for higher H_2 content in the gas mixture: both quantities first decrease (here from 1 bar to 10 bar) then increase (here from 10 bar to 20 bar) for the considered temperature range. For the pure H_2-air mixture, as explained in Zhao et al. (2011), such non-monotonic behavior is due to the competition between the chain branching reactions (e.g. $H+O_2=O+OH$ and $H_2O_2+M=2OH+M$) and the chain termination reaction (e.g. $H+O_2+M=HO_2+M$) which strongly depend on the high pressure. The key chemical reactions for the NH_3-H_2-air gas mixtures with higher H_2 content (here higher than 30%) to explain such non-monotonic behavior at high pressures, to author's knowledge, has not yet been intensively reported, which is beyond the scope of this work and requires further study @Bo: Is this correct? @Chunkan: in the case that hydrogen content is more than 30 percent, the hydrogen ignition will dominate the whole chemistry, i.e, the explanation for hydrogen-air mixture can be adopted for ammonia-hydrogen mixture. However, concerning the process safety, at higher pressures, the pre-heated NH_3-H_2-air mixtures with higher H_2 content are as easily self-ignited as pre-heated pure H_2-air gas mixture under higher strain rates (similar order of magnitude of a_{trans} and $k(T_{ub})$).

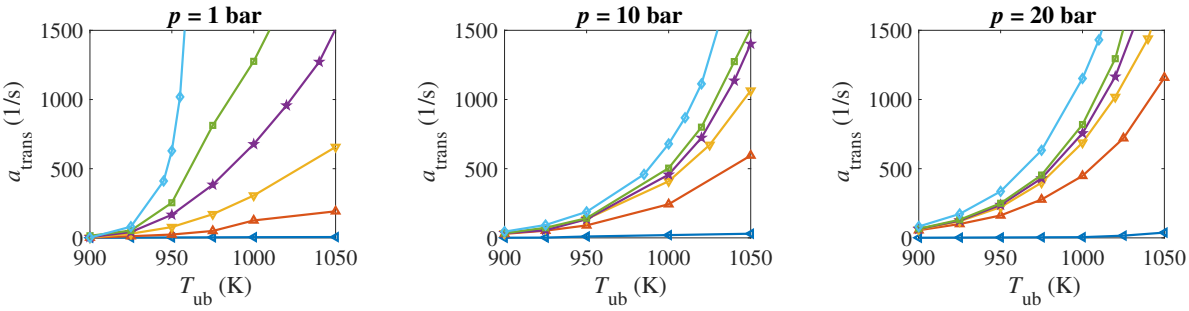

Figure 12: Dependence of the a_{trans} over the gas mixture temperature T_{ub} for three different pressures. The color lines are the same as in Fig.6.

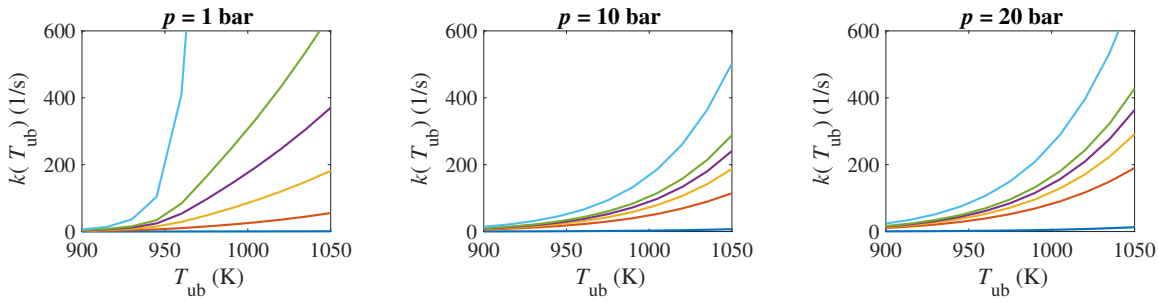

Figure 13: Dependence of the characteristic reaction rate $k(T_{ub})$ over the gas mixture temperature T_{ub} for three different pressures. The color lines are the same as in Fig.6.

Since the tendency of a_{trans} corresponds to the one of $k(T_{ub})$, Fig.14 shows the a_{trans} against the characteristic reaction rate $k(T_{ub})$. It is observed that there exists a quasi-linear correlation, and the linear regression model gives the

relationship between the transition strain rate a_{trans} and the characteristic reaction rate $k(T_{ub}) = 1/\tau_{ign}$ as

$$a_{trans} \approx 4.545 \cdot k(T_{ub}) \approx \frac{4.545}{\tau_{ign}}. \tag{7}$$

If the reaction rate tends to zero ($k \to 0$), corresponding to an infinite reaction time, the gas mixture cannot also be self-ignited and $a_{trans} \to 0$.

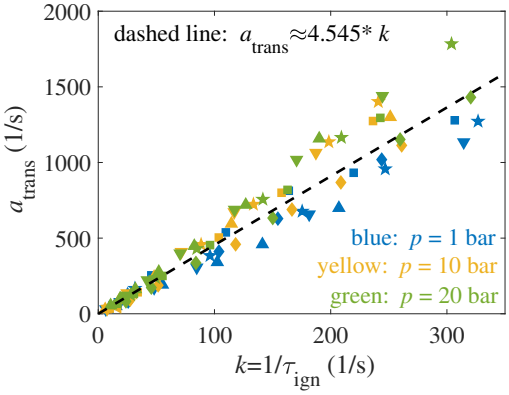

Figure 14: Correlation between a_{trans} and characteristic reaction rate $k = 1/\tau_{ign}$ for various mixture compositions and pressures. ◀: pure NH_3; ▲: NH_3:H_2=0.9:0.1; ▼: NH_3:H_2=0.8:0.2; ★: NH_3:H_2=0.7:0.3; ■: NH_3:H_2=0.6:0.4; ♦: pure H_2.

This simple linear correlation provides the information that if one knows the ignition delay time of the gas mixture at one temperature, the transition strain rate a_{trans} can be easily determined. Hence, for the process safety, if the gas mixture is pre-heated, one can easily estimate the critical strain rate, under which the gas mixture can be self-ignited.

4. Conclusion

The following issues are suggested to be discussed in the future:

- How large different chemical mechanisms?
- Whether using different chemical mechanisms also give the same correlation?

5. Acknowledgements

References

Abbas, H., Daud, W., 2010. Hydrogen production by methane decomposition: a review. International Journal of Hydrogen Energy 35(3), 1160–1190.

Božo, M.G., Vigueras-Zuniga, M., Buffi, M., Seljak, T., Valera-Medina, A., 2019. Fuel rich ammonia-hydrogen injection for humidified gas turbines. Applied Energy 251, 113334.

Bradley, D., Lung, F.K.K., 1987. Spark ignition and the early stages of turbulent flame propagation 69, 71–93.

Cesaro, Z., Ives, M., Nayak-Luke, R., Mason, M., Bañares-Alcántara, R., 2021. Ammonia to power: Forecasting the levelized cost of electricity from green ammonia in large-scale power plants. Applied Energy 282, 116009.

Colson, S., Hayakawa, A., Kudo, T., Kobayashi, H., 2016. Extinction characteristics of ammonia/air counterflow premixed flames at various pressures. Journal of Thermal Science and Technology 11, JTST0048–JTST0048.

De Soete, G., 1971. The influence of isotropic turbulence on the critical ignition energy, in: Symposium (International) on Combustion, Elsevier. pp. 735–743.

Essmann, S., Markus, D., Grosshans, H., Maas, U., 2020. Experimental investigation of the stochastic early flame propagation after ignition by a low-energy electrical discharge 211, 44–53.

Goldmann, A., Dinkelacker, F., 2021. Experimental investigation and modeling of boundary layer flashback for non-swirling premixed hydrogen/ammonia/air flames. Combustion and Flame 226, 362–379.

Han, X., Wang, Z., Costa, M., Sun, Z., He, Y., Cen, K., 2019a. Experimental and kinetic modeling study of laminar burning velocities of nh3/air, nh3/h2/air, nh3/co/air and nh3/ch4/air premixed flames. Combustion and Flame 206, 214–226.

Han, X., Wang, Z., Costa, M., Sun, Z., He, Y., Cen, K., 2019b. Experimental and kinetic modeling study of laminar burning velocities of nh3/air, nh3/h2/air, nh3/co/air and nh3/ch4/air premixed flames. Combustion and Flame 206, 214–226. 10.1016/j.combustflame.2019.05.003.

Hayakawa, A., Goto, T., Mimoto, R., Arakawa, Y., Kudo, T., Kobayashi, H., 2015a. Laminar burning velocity and markstein length of ammonia/air premixed flames at various pressures. Fuel 159, 98–106. 10.1016/j.fuel.2015.06.070.

Hayakawa, A., Goto, T., Mimoto, R., Arakawa, Y., Kudo, T., Kobayashi, H., 2015b. Laminar burning velocity and markstein length of ammonia/air premixed flames at various pressures. Fuel 159, 98–106.

Hirschfelder, J.O., Curtiss, C.F., Bird, R.B., Mayer, M.G., 1964. Molecular theory of gases and liquids. volume 165. Wiley New York.

Huang, C., Shy, S., Liu, C., Yan, Y., 2007. A transition on minimum ignition energy for lean turbulent methane combustion in flamelet and distributed regimes. Proceedings of the Combustion Institute 31, 1401–1409.

Ichikawa, A., Hayakawa, A., Kitagawa, Y., Kunkuma Amila Somarathne, K.D., Kudo, T., Kobayashi, H., 2015. Laminar burning velocity and markstein length of ammonia/hydrogen/air premixed flames at elevated pressures. Int. J. Hydrogen Energy 40, 9570–9578. 10.1016/j.ijhydene.2015.04.024.

Kumar, P., Meyer, T.R., 2013. Experimental and modeling study of chemical-kinetics mechanisms for h2–nh3–air mixtures in laminar premixed jet flames. Fuel 108, 166–176. 10.1016/j.fuel.2012.06.103.

Lee, S., Kwon, O.C., 2011. Effects of ammonia substitution on extinction limits and structure of counterflow nonpremixed hydrogen/air flames. International Journal of Hydrogen Energy 36, 10117–10128. 10.1016/j.ijhydene.2011.05.082.

Lhuillier, C., Brequigny, P., Lamoureux, N., Contino, F., Mounaïm-Rousselle, C., 2020. Experimental investigation on laminar burning velocities of ammonia/hydrogen/air mixtures at elevated temperatures. Fuel 263, 116653. 10.1016/j.fuel.2019.116653.

Li, J., Lai, S., Chen, D., Wu, R., Kobayashi, N., Deng, L., Huang, H., 2021. A review on combustion characteristics of ammonia as a carbon-free fuel. Frontiers in Energy Research 9. 10.3389/fenrg.2021.760356.

Li, R., Konnov, A.A., He, G., Qin, F., Zhang, D., 2019. Chemical mechanism development and reduction for combustion of nh3/h2/ch4 mixtures. Fuel 257, 116059.

Livengood, J., Wu, P., 1955. Correlation of autoignition phenomena in internal combustion engines and rapid compression machines. Symposium (International) on Combustion 5, 347–356.

Maas, U., Raffel, B., Wolfrum, J., Warnatz, J., 1988. Observation and simulation of laser induced ignition processes in o2- o3 and h2- o2 mixtures. Symposium (International) on Combustion 21, 1869–1876.

Maas, U., Warnatz, J., 1988. Ignition processes in hydrogen oxygen mixtures. Combustion and flame 74, 53–69.

Mashruk, S., Vigueras-Zuniga, M.O., Tejeda-del Cueto, M.E., Xiao, H., Yu, C., Maas, U., Valera-Medina, A., 2022. Combustion features of ch4/nh3/h2 ternary blends. International Journal of Hydrogen Energy .

Ronney, P.D., 1988. Effect of chemistry and transport properties on near-limit flames at microgravity. Combustion Science and Technology 59, 123–141.

Shy, S., Shiu, Y., Jiang, L., Liu, C., Minaev, S., 2017. Measurement and scaling of minimum ignition energy transition for spark ignition in intense isotropic turbulence from 1 to 5 atm. Proceedings of the Combustion Institute 36, 1785–1791.

Stahl, G., Warnatz, J., 1991. Numerical investigation of time-dependent properties and extinction of strained methane- and propane-air flamelets. Combustion and flame 85, 285–299.

Valera-Medina, A., Gutesa, M., Xiao, H., Pugh, D., Giles, A., Goktepe, B., Marsh, R., BOWEN, P., 2019. Premixed ammonia/hydrogen swirl combustion under rich fuel conditions for gas turbines operation. International Journal of Hydrogen Energy 44, 8615–8626.

Valera-Medina, A., Xiao, H., Owen-Jones, M., David, W., Bowen, P.J., 2018. Ammonia for power. Progress in Energy and Combustion Science 69, 63–102. 10.1016/j.pecs.2018.07.001.

Wang, S., Wang, Z., Elbaz, A.M., Han, X., He, Y., Costa, M., Konnov, A.A., Roberts, W.L., 2020. Experimental study and kinetic analysis of the laminar burning velocity of nh3/syngas/air, nh3/co/air and nh3/h2/air premixed flames at elevated pressures. Combustion and Flame 221, 270–287.

Wiseman, S., Rieth, M., Gruber, A., Dawson, J.R., Chen, J., 2021. A comparison of the blow-out behavior of turbulent premixed ammonia/hydrogen/nitrogen-air and methane–air flames. Proc. Comb. Inst. 38, 2869–2876.

Yin, G., Wang, C., Zhou, M., Zhou, Y., Hu, E., Huang, Z., 2022. Experimental and kinetic study on laminar flame speeds of ammonia/syngas/air at a high temperature and elevated pressure. Frontiers in Energy 16, 263–276. 10.1007/s11708-021-0791-7.

Zhao, Z., Chen, Z., Chen, S., 2011. Correlations for the ignition delay times of hydrogen/air mixtures. Chinese Science Bulletin 56, 215–221.